RESEARCH PAPER

PCCP
www.rsc.org/pccp

Orientation and conformation of octadecyl rhodamine B in hybrid Langmuir–Blodgett monolayers containing clay minerals

Robin H. A. Ras,[a] József Németh,[ab] Cliff T. Johnston,[c] Imre Dékány[b] and Robert A. Schoonheydt*[a]

[a] *Centrum voor Oppervlaktechemie en Katalyse, K.U.Leuven, Kasteelpark Arenberg 23 B-3001 Leuven, Belgium. E-mail: robert.schoonheydt@agr.kuleuven.ac.be*
[b] *Department of Colloid Chemistry, University of Szeged, Aradi V. t. 1., H-6720 Szeged, Hungary*
[c] *Birck Nanotechnology Center, 915 W. State Street, 1150 Lilly Hall, Purdue University West Lafayette, IN 47907-2054, USA*

Received 17th May 2004, Accepted 17th September 2004
First published as an Advance Article on the web 11th October 2004

To control the molecular organization of octadecyl rhodamine B (RhB18), hybrid Langmuir–Blodgett monolayers containing clay minerals were prepared. The orientation and conformation of the RhB18 molecule were analyzed by polarized attenuated total reflection Fourier transform infrared (ATR–FTIR) spectroscopy and fluorescence spectroscopy. Monomers and dimers of RhB18 were observed by UV-Vis absorption spectroscopy. Infrared bands of RhB18 exhibited dichroism and shifted to higher or lower wavenumbers in films as a function of clay content. The main fluorescence band of RhB18 was more intense and shifted to lower wavelengths in films with higher clay content. In films without clay, the phenyl group of RhB18 is tilted relative to the xanthene group and both groups are tilted relative to the substrate. In films with clay, both the phenyl group and xanthene group are oriented parallel to the clay surface which is parallel to the substrate. The clay mineral surface induces a change in the conformation and orientation of the RhB18 chromophore.

1. Introduction

Materials containing dye molecules are of considerable interest from a fundamental point of view as well as for potential applications.[1,2] The photophysical properties of such materials are sensitive to the spatial organization of the dye molecules, *i.e.* the density of molecules as well as their mutual orientation. In a photophysical process, energy is put into a molecule by absorption of light and as a consequence, the electronically excited molecule may experience changes in the quantum states concomitant with the exchange of energy (*e.g.*, fluorescence, resonance energy transfer). By controlling the spatial organization of dye molecules, one can control the photophysical properties.

One approach to control the spatial organization of dye molecules is to adsorb them on surfaces. The surfaces that have been investigated regarding the orientational organization comprise intercalation compounds (*e.g.*, interlamellar regions of clay minerals,[3–9] $K_4Nb_6O_{17}$,[10] aluminium oxide[11]) and flat substrates (*e.g.*, external surfaces of clay minerals,[12,13] gold,[14] water,[15,16] glass/quartz[17–20]). The orientation of dye molecules adsorbed on surfaces has been determined using one or a combination of the following techniques: X-ray diffraction,[5–7,9,10] polarized ultraviolet-visible (UV-Vis) spectroscopy,[6,10,12,17,19,20] fluorescence spectroscopy,[16] molecular modeling,[9] scanning tunneling microscopy,[14] second harmonic generation,[13,15–18] near edge X-ray absorption fine structure spectroscopy[21] and polarized transmission infrared spectroscopy.[6–8]

Smectite clay minerals are silicate materials that consist of *ca.* 1 nm thick lamellae. These lamellae are made of one sheet of edge-linked Al or Mg octahedra sandwiched between two sheets of corner-linked Si tetrahedra. The corners of the octahedra and tetrahedra are oxygen atoms. Isomorphic substitution induces negative charges in the clay lamella and for charge compensation reasons, cations (*e.g.*, Na^+) are adsorbed on the clay mineral surface. These cations can be exchanged by organic cations to form organo-clay complexes. For long-chain alkylammonium cations, the conformation of the alkyl chain depends on the surface charge density of the clay mineral and on the alkyl chain length.[22,23] Cationic dye molecules are found with their chromophoric group parallel or tilted to the clay surface depending on the surface charge density of the clay mineral.[5,6,8,21] The layered structure and the cation-exchange properties of clay minerals make them interesting as host materials for dye molecules.

The Langmuir–Blodgett (LB) method provides a novel approach to assembling and manipulating single lamellae of clay particles and dye monolayers. Unlike prior work on dye–clay materials, this approach offers a high level of control on the organization of both dye molecules and clay mineral particles. LB monolayers containing octadecyl rhodamine B (RhB18) and clay minerals have been reported recently.[24] The LB films are prepared by spreading a chloroform solution of RhB18 on the surface of a dilute aqueous dispersion of the smectite clay under investigation. As the clay concentration in the dispersion increases from 0 to 50 mg dm^{-3}, gradually more clay mineral lamellae are built in the monolayer until a pure hybrid monolayer is obtained, consisting of one layer of clay mineral lamellae of *ca.* 1 nm thickness and one monolayer of RhB18 on top of it.[24] The density of RhB18 molecules in the film is largely determined by the surface charge density of the clay mineral.[24] Above 50 mg dm^{-3} clay concentrations, films containing aggregates of clay particles are formed at the air–water interface. The density of RhB18 molecules in these films is smaller than in the pure hybrid monolayer obtained at clay concentrations of 50 mg dm^{-3}.

DOI: 10.1039/b411339j

In this paper we investigate the spatial organization of RhB18 in hybrid clay monolayers by focusing on the orientation of the molecules using polarized attenuated total reflection Fourier transform infrared spectroscopy and fluorescence spectroscopy.

2. Materials and methods

2.1. Materials

The clay mineral species used in this work was saponite (SapCa-1) obtained from the Source Clays Repository of the Clay Minerals Society. The clay was Na^+ saturated by repeated (three times) exchange with 1 M NaCl solutions followed by dialysis with water until a negative Cl^- test was obtained using $AgNO_3$. The particle size fraction between 0.5 and 2.0 μm was obtained by centrifugation and freeze-drying of a salt-free, Na^+ exchanged clay dispersion. The elemental composition of half a unit cell was determined by XRD analysis: $[(Si^{4+}{}_{3.57}\ Al^{3+}{}_{0.38}\ Fe^{3+}{}_{0.05})\ (Mg^{2+}{}_{3.00})\ O_{10}(OH)_2]\ Na^+{}_{0.43}$.

Octadecyl rhodamine B chloride (RhB18, Molecular Probes) was used as received and was dissolved in HPLC grade chloroform (99.9%, Aldrich, stabilized by 0.5–1% ethanol) to prepare a spreading solution of 9.11×10^{-4} mol dm^{-3}.

2.2. Langmuir–Blodgett film preparation

LB films were prepared on a NIMA Technology model 611 LB trough at a temperature of 23 ± 1 °C. Clay dispersions stirred for 24 h in Milli-Q water were used as subphase. The clay concentration ranged from 2 to 250 mg dm^{-3}. A microsyringe was used to spread 40 μl of the dye dissolved in chloroform over the subphase. After 15 min, the film was compressed at a rate of 30 cm^2 min^{-1}. Films were deposited in upstroke (lifting speed of 5 mm min^{-1}) at surface pressures of 2 mN m^{-1} and 15 mN m^{-1} on ZnSe internal reflection elements (IREs) for infrared spectroscopy and on glass substrates for UV-Vis absorption and fluorescence spectroscopies. The IREs were cleaned prior to each deposition by gently rubbing with a paper tissue soaked in methanol. The glass substrates were treated in piranha solution (mixture of 70 ml concentrated H_2SO_4 and 30 ml 35% H_2O_2) for 30 min at 90 °C. Subsequently the glass substrates were thoroughly rinsed by deionized water and stored in Milli-Q water no longer than 30 d.

2.3. Infrared spectroscopy

The IREs were ZnSe trapezoidal-shaped crystals (Spectroscopy Central, UK) (50 × 20 × 2 mm) with 25 internal reflections and were measured in a vertical ATR cell using a Bruker IFS66v/S vacuum FTIR spectrometer with an operating vacuum lower than 3 mbar inside the spectrometer. Because the IRE was not covered with film where it was attached to the dipper, there are only 24 active reflections. Polarized ATR–FTIR spectra were obtained using a wire-grid polarizer. The FTIR spectrometer was equipped with a liquid nitrogen cooled MCT detector and a KBr/Ge beam splitter. A total of 512 scans were signal averaged using an optical resolution of 2 cm^{-1}. Spectra were analyzed with Grams/32 AI Version 6.00 software.

2.4. UV-Vis absorption spectroscopy

UV-Vis absorption spectra of the monolayers on glass substrates were measured from 400 nm to 700 nm on a Perkin Elmer Lambda 12 spectrometer. A clean glass slide was used as reference.

2.5. Fluorescence spectroscopy

Fluorescence spectra were taken on a SPEX Fluorolog 3–22 double grating fluorescence spectrometer (Jobin Yvon). The samples were excited at 550 nm and the fluorescence light was collected from the sample surface at an angle of 22.5° to the excitation light (front-face geometry).

3. Results

3.1. Infrared spectroscopy

Attenuated total reflection Fourier transform infrared (ATR–FTIR) spectra of RhB18 monolayers prepared on water and on a saponite dispersion are shown in Fig. 1 together with the transmission infrared (IR) spectrum of RhB18 in KBr. The strongest features in the spectrum of the hybrid film (Fig. 1a) are the clay mineral Si–O stretching bands, ν(Si–O), in the 900 cm^{-1} to 1120 cm^{-1} region and have recently been discussed in detail.[25,26]

The IR spectrum of RhB18 (Fig. 1) shows a complex suite of bands in the 700 to 1800 cm^{-1} region, typical of rhodamine-type dyes. Despite many IR studies on RhB derivatives[7,9,19,27,28] and other xanthene dyes[29–31] (xanthene = $C_{13}H_{10}O$ tricyclic structure; see Fig. 8) have been reported, the assignment of the majority of IR bands remains unclear. This is due, in part, to the size of the molecule that is too large for detailed vibrational analysis using first principle methods. RhB18 consists of 51 non-H atoms (118 atoms including H) and this corresponds to 348 IR- or Raman-active bands (3N-6). From an experimental perspective, vibrational assignments require IR data collected from isotopic derivatives (*i.e.*, RhB18 synthesized using ^{13}C, ^{2}H, ^{18}O, and/or ^{15}N) and these compounds have not been synthesized. However, the following three bands have been assigned unambiguously. The band at 1724 cm^{-1} has been assigned to the carbonyl stretch, ν(C=O) of the ester group.[9,27,28,31] The band at 1590 cm^{-1} has been assigned to the in-plane CC skeletal stretching vibration.[7,9,19,27–29,31] The band at 808 cm^{-1} has been assigned to the out-of-plane aromatic CH bending.[29,31–34] For the other bands in the spectral region from 1800 to 700 cm^{-1}, there is no agreement for their assignment in the literature.

Dichroic ratio of IR bands of RhB18

The dichroic ratio (DR = A_s/A_p) of the in-plane CC skeletal stretching vibration of RhB18 near 1590 cm^{-1} is plotted against the s-polarized intensity of the Si–O stretch at 996 cm^{-1} in Fig. 2. The intensity of the Si–O stretch is a measure for the

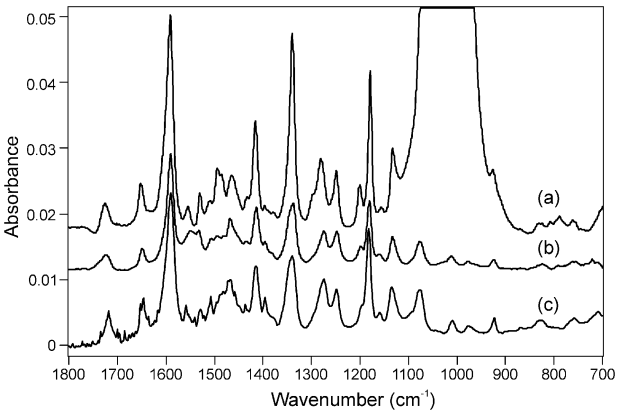

Fig. 1 Infrared spectra in the region 1800–700 cm^{-1}. (a) p-Polarized ATR spectrum of RhB18 monolayer prepared on a 50 mg dm^{-3} saponite dispersion deposited at 15 mN m^{-1}; (b) p-polarized ATR spectrum of RhB18 monolayer prepared on water deposited at 15 mN m^{-1}; (c) transmission spectrum of RhB18 in KBr. The absorbance values in the *y*-axis are valid for the ATR spectra (a) and (b).

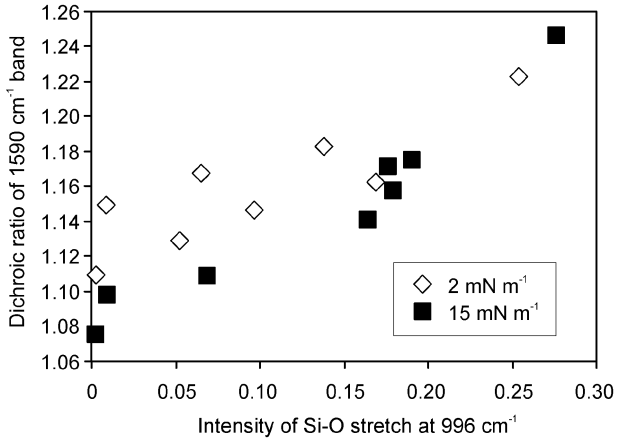

Fig. 2 Dichroic ratio ($DR = A_s/A_p$) of the most intense infrared band of RhB18 near 1590 cm^{-1} as a function of the ATR–FTIR intensity of the Si–O stretch at 996 cm^{-1} of RhB18 hybrid monolayers prepared on saponite dispersions with varying clay concentrations at surface pressures of 2 and 15 mN m^{-1}. The intensity of the Si–O stretch at 996 cm^{-1} is a measure for the clay content in the film.

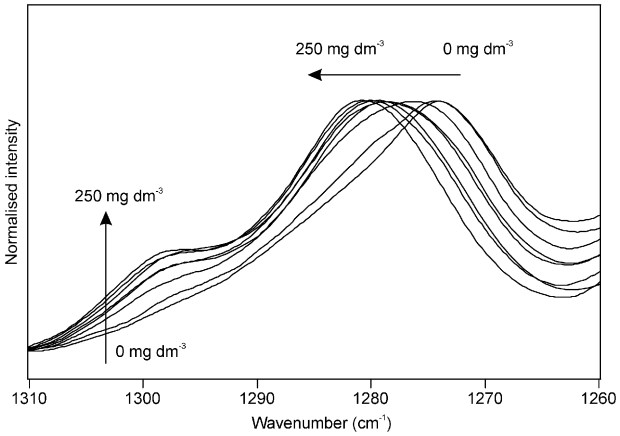

Fig. 4 ATR–FTIR spectrum (s-polarization) from 1310 to 1260 cm^{-1} of RhB18–saponite films prepared on dispersions with varying clay concentration deposited at 2 mN m^{-1}. The band near 1280 cm^{-1} shifts to higher wavenumber and a band near 1300 cm^{-1} appears when the clay content in the film increases.

amount of clay mineral in the film.[24] One observes an increase of the dichroic ratio with increasing intensity of the Si–O stretch, or with the amount of clay mineral. Because the 1590 cm^{-1} band is assigned to a vibration in the plane of the RhB18 chromophore, it indicates that for the film prepared on water the chromophore plane changes from a tilted orientation with respect to the substrate to an orientation parallel to the substrate for the films having clay. As the clay particles in the film are oriented parallel to the substrate,[25,26] it shows that the chromophore plane is parallel to the clay surface as well. The trend in Fig. 2 is also observed for the bands at 1415, 1339, 1280, 1248 and 1178 cm^{-1}, indicating that these bands are associated with the chromophore plane.

The out-of-plane aromatic CH bending mode is observed at 808 cm^{-1} in the p-polarized spectra of the clay films (Fig. 3). The presence of this band in the p-polarized spectrum and its absence in the s-polarized spectrum confirms that the chromophore is oriented parallel to the clay surface. The band is not visible in the p- and s-polarized spectra of the RhB18 monolayer prepared on water giving evidence for the non-parallel orientation of the chromophore in films without clay.

Shift of IR bands of RhB18

The RhB18 bands at 1590, 1415, 1339, 1280 and 1248 cm^{-1} shift to higher wavenumbers for the films prepared on dispersions with increasing clay concentration. An example is shown in Fig. 4 for the band near 1280 cm^{-1}. It shifts from 1274 cm^{-1} in films without clay to 1281 cm^{-1} for films in the presence of clay. The chromophore band at 1178 cm^{-1} shifts to lower wavenumbers for the films prepared on dispersions with increasing clay concentration. Also new bands appear, for example near 1300 cm^{-1} (Fig. 4). To the best of our knowledge, a shift of IR bands of rhodamine compounds has not yet been observed.

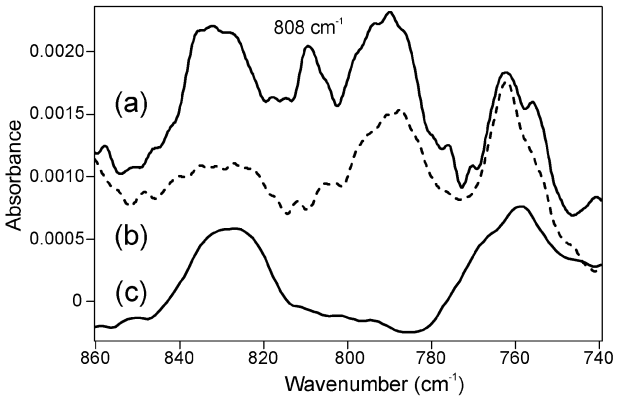

Fig. 3 (a) p- and (b) s-polarized ATR–FTIR spectra of the RhB18 monolayer prepared on a 50 mg dm^{-3} saponite dispersion at a surface pressure of 2 mN m^{-1}. (c) Transmission FTIR spectrum of RhB18 in a KBr pellet. The band at 808 cm^{-1} in the p-polarized ATR-FTIR spectrum is assigned to the out-of-plane aromatic CH bending mode.

3.2. UV-Visible absorption spectroscopy

UV-Visible absorption spectra of RhB18–saponite monolayers deposited on glass at 2 mN m^{-1} are shown in Fig. 5a. The absorbance increases and the absorption maximum shifts gradually with increasing clay concentration from 568 nm for films prepared on water, to 580 nm for films prepared on a 50 mg dm^{-3} clay dispersion. Films made at still higher clay concentration (250 mg dm^{-3}) have the absorption maximum at 571 nm. The band shift is indicative of several species contributing to the spectrum, or for a change, in the polarity of the local environment at the clay mineral surface. Although we cannot exclude an effect of local environment variations, the following results support the hypothesis for the presence of monomer species and dimer species of RhB18.[24]

The RhB18 UV-Vis spectra of Fig. 5a can be decomposed into 3 components (see Appendix): the spectrum of the monomer with maximum at 567 nm, that of a H-dimer with maximum around 540 nm and that of a J-dimer with maximum around 583 nm. When the monomer spectrum is subtracted from the measured spectrum, the spectra of the dimers are obtained (the subtraction method is explained in the Appendix). These dimer spectra are shown in Fig. 5b.

One can observe a relatively weak, broad band around 540 nm, and a band with varying intensity around 583 nm. These two bands are assigned to, respectively, H-dimers with a sandwich-type of geometry and to J-dimers with a linear-type of geometry.[35] Band splitting occurs for dimers with an intermediate geometry.[36] From the increase of the band at 583 nm (Fig. 5b) can be concluded that mainly J-dimers and no H-dimers are added in the films when the clay concentration of the dispersion is increased up to 50 mg dm^{-3}. In a previous paper[24] was shown that these films also contain an increasing amount of clay lamellae and RhB18 molecules to reach a maximum at 50 mg dm^{-3} clay concentration. Further increase in clay concentration (250 mg dm^{-3}) results in clay aggregates and lower RhB18 density.[24] Integration of the spectra from 450

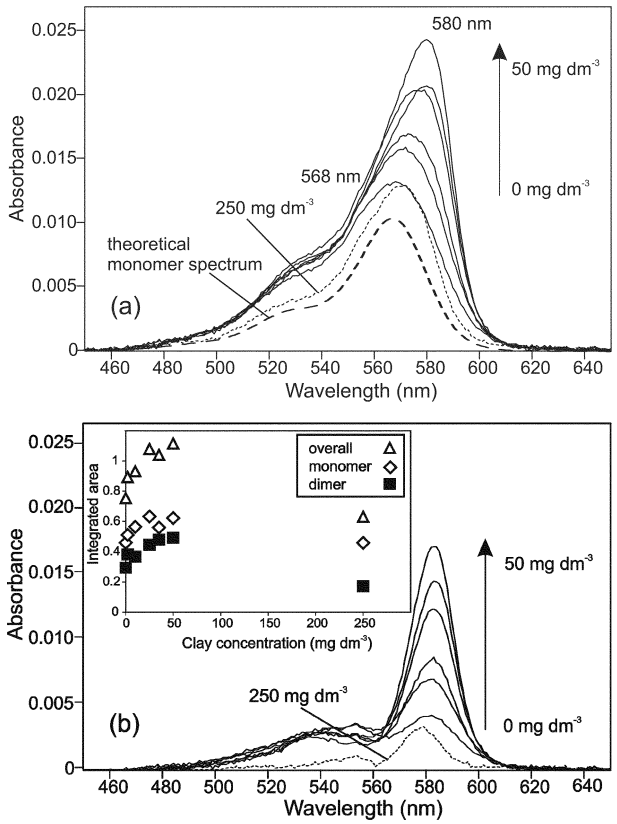

Fig. 5 (a) UV-Vis absorption spectra and (b) calculated dimer spectra of RhB18–saponite films prepared on dispersions with increasing clay concentration deposited at a surface pressure of 2 mN m^{-1}. The dimer spectra are obtained by subtraction of the theoretical monomer spectrum (a) according to the method described in the Appendix. The figure in the inset of (b) shows the amount of monomers and dimers in the films expressed as the integrated area under the spectrum from 450 to 650 nm.

to 650 nm allows the quantification of the relative amount of monomers and dimers in the films. The integrated areas of the monomer and dimer spectra are plotted in the inset of Fig. 5b. The amount of monomers in the film (white diamonds) increases together with the amount of dimers (black squares) up to a clay concentration of about 50 mg dm^{-3}. Further increase in clay concentration (250 mg dm^{-3}) results in only a slightly lower amount of monomers, but a significantly lower amount of dimers.

3.3. Fluorescence spectroscopy

Fluorescence spectra of RhB18–saponite monolayers deposited at 2 mN m^{-1} are shown in Fig. 6. The most intense

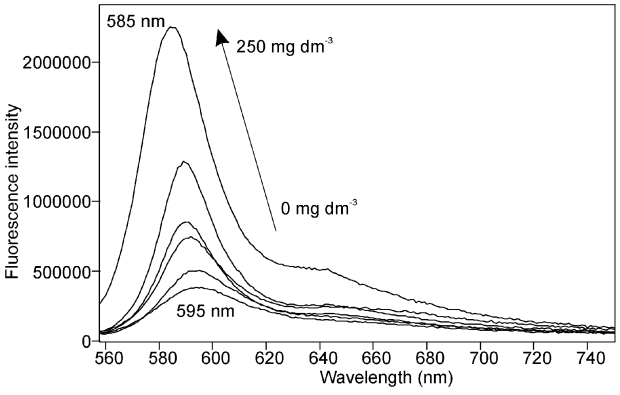

Fig. 6 Fluorescence spectra of RhB18–saponite films prepared on dispersions with increasing clay concentration deposited at a surface pressure of 2 mN m^{-1} (excitation at 550 nm).

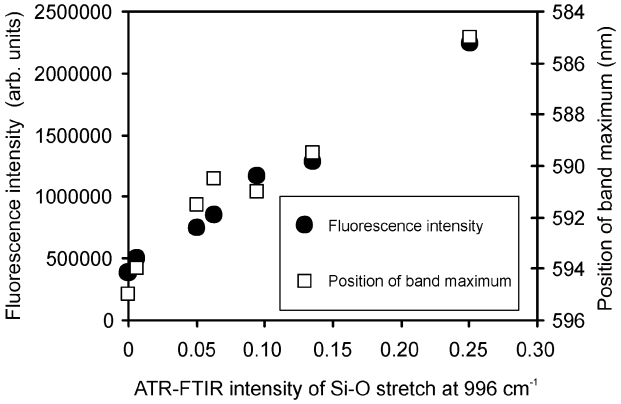

Fig. 7 Fluorescence intensity and position of the fluorescence band maximum of RhB18–clay monolayers deposited at 2 mN m^{-1} plotted as a function of the ATR–FTIR intensity of the Si–O stretch at 996 cm^{-1}, which is a measure for the amount of clay in the film.

fluorescence band is attributed to monomers.[37] The shoulder near 640 nm is attributed to weakly fluorescent J-dimers.[37] These observations agree with the UV-Visible absorption spectra, which show the presence of mainly monomers and J-dimers. Two trends can be observed with increasing clay concentration: a blue-shift of the fluorescence maximum (from 595 nm for the film prepared on water, to 585 nm for the film prepared on a 250 mg dm^{-3} clay dispersion) and an increase in the fluorescence intensity. These two trends are also observed in the fluorescence spectra of the films prepared at a surface pressure of 15 mN m^{-1} (not shown). When the fluorescence intensity and the position of the band maximum of the monomer are plotted as a function of the ATR–FTIR intensity of the Si–O stretch at 996 cm^{-1}, one observes an almost linear increase for both features (Fig. 7). This suggests that the same mechanism causes the shift of these two features. The ATR–FTIR intensity of the Si–O stretch at 996 cm^{-1} is a measure for the amount of clay in the film.[24] It indicates that the monomer fluorescence is largely associated with RhB18 adsorbed at the clay mineral surface.

3. Discussion

After spreading RhB18 surfactant molecules on a clay mineral dispersion, a hybrid clay film is formed at the air/water interface. The molecular density and the density of clay particles were analyzed in a recent publication[24] and a formation mechanism of these hybrid clay mineral films was proposed. The molecular density was found to be determined by the surface charge density of the clay mineral.[24] The results from the present paper suggest that the clay mineral surface not only influences the molecular density, but also the orientation and the conformation of the rhodamine molecules.

The dichroic ratio of both the in-plane and out-of-plane vibrational modes of RhB18 in the hybrid LB film indicate that RhB18 is oriented with the plane of the rings parallel to the 001 surface of the clay mineral. The 1590 cm^{-1} band is assigned to an in-plane CC skeletal stretching vibration.[9,27,28,31] The increase of its dichroic ratio indicates that more and more molecules are oriented with their molecular plane parallel to the clay mineral surface. Additional support for the preferred orientation of the RhB18 chromophore is provided by the dichroic ratio of the out-of-plane aromatic CH bending band at 808 cm^{-1} which is only present in the p-polarized spectra of the hybrid clay films (Fig. 3). This behaviour is consistent with earlier studies of aromatic molecules at the smectite clay surface where an orientation parallel to the 001-plane is observed.[5,8,38–40] Studies of chromophores in monolayers prepared on water show tilted orientations.[15,17]

The blue shift of the fluorescence maximum and the concomitant increase in fluorescence intensity (Figs. 6 and 7) have been described before for monolayers containing rhodamine dye molecules.[15,37,41–43] In those papers it was suggested that a conformational change of the monomer is responsible for a distribution of energy levels.[15,37,41–43] The conformational change corresponds to different tilt angles of the phenyl ring relative to the xanthene plane (Fig. 8).[15,37,41–43]

Pospíšil *et al.*[9] have calculated that in vacuum the conformation of RhB with the lowest energy corresponds to the phenyl ring perpendicular to the xanthene plane. In LB films prepared on water, in the absence of clay mineral particles, a range of monomer conformations exists with various angles between the phenyl ring and the xanthene plane.[16,37,41] When a RhB18 monomer is excited, its excitation energy migrates *via* neighbouring monomers to the monomers of lower energy (Fig. 8) [15,37,41–43] Consequently, in films prepared on water mainly low-energy monomers have collected the excitation energy resulting in fluorescence with a band maximum at 595 nm. During the migration of energy, quenching of fluorescence occurs resulting in a lower fluorescence intensity. Moreover, dimers can act as efficient traps for excitation energy.

In films containing clay minerals, there is a blue-shift and an increase in intensity compared to the film prepared on water. The blue-shift and the intensity increase are proportional to the clay content in the film (Fig. 7). Thus, more high-energy RhB18 monomers are present as more clay mineral particles are incorporated in the LB films. The conformation of a high-energy RhB18 monomer adsorbed on the clay surface is with the phenyl ring parallel to the xanthene plane (see Fig. 8).

The inset of Fig. 5b shows that the maximum amount of monomers in the film is reached at a clay concentration of about 50 mg dm^{-3}. This should correspond to a maximum in fluorescence intensity and to a maximum in band shift. The maximum in fluorescence intensity and the maximum in band shift, however, are observed for films prepared on 250 mg dm^{-3} clay dispersions. This is in agreement with the data in Fig. 5b which indicate that such films mainly contain monomers and almost no H- or J-dimers.

A second explanation reported in literature for the observed band shift in the absorption and fluorescence spectra is a change in the polarity or acidity of the local environment.[44] The clay mineral surface contains heterogeneous adsorption sites that provide different local environments for the RhB18 molecules than the water or glass surface. Although we cannot exclude the latter hypothesis, the UV-Vis spectra and the calculated dimer spectra (Fig. 5) support the presence of monomer and dimer species of RhB18. In addition, two independent analytical techniques (polarized infrared spectroscopy and fluorescence spectroscopy) support the hypothesis for the conformational change of RhB18 monomers. In films without clay, the phenyl group of RhB18 is tilted relative to the xanthene group and both groups are tilted relative to the substrate. In films with clay, both the phenyl group and xanthene group are oriented parallel to the clay surface which is parallel to the substrate.

From the conclusions on the RhB18 conformation in the films, a possible explanation can be proposed for the observed shift of the IR bands (Fig. 4). To the best of our knowledge, a shift of IR bands of rhodamine compounds has not yet been observed. Recently, Kato *et al.* observed a shift of some IR bands of a merocyanine dye during a phase transition.[45] Takayanagi *et al.* observed that upon irradiation of a merocyanine dye the relative intensity of some IR bands varies.[46] Both observations have been related to a change in the conformation of the molecule.[45,46] Similarly, we can relate the IR band shift near 1590, 1415, 1339, 1280, 1248 and 1178 cm^{-1} (Fig. 4) to a change in the conformation of RhB18 in hybrid clay films. The IR band shift and the appearance of new bands coincide with the higher clay content in the film,[24] with the observed changes in dichroic ratio (Figs. 2 and 3) and with the changes in fluorescence properties (Figs. 6 and 7). Therefore, the IR band shift and the appearance of new bands can be attributed to adsorption of RhB18 onto the clay surface giving a conformational change, as shown in Fig. 8.

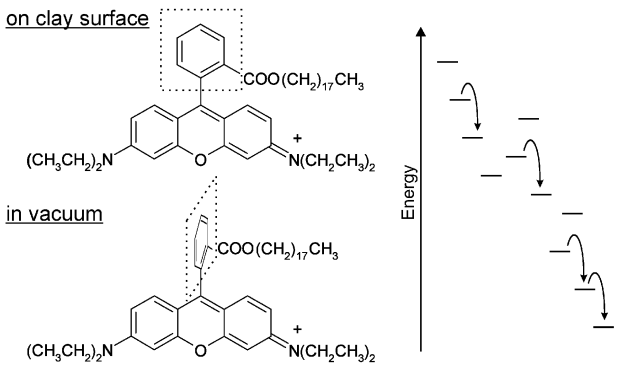

Fig. 8 Structure of RhB18 showing the tilt of the phenyl ring with respect to the xanthene plane. The xanthene plane is drawn in the plane of the paper. The tilt of the phenyl ring causes a distribution in the energy level of RhB18 monomers. The conformation in vacuum has the lowest energy and corresponds to the phenyl ring perpendicular to the xanthene plane.[9] The conformation on the clay mineral surface has a high energy and corresponds to the phenyl ring parallel to the xanthene plane. At the water surface the phenyl ring can adopt various angles relative to the xanthene plane. Thus, monomers with various energy levels are present at the water surface. When RhB18 is excited, the excitation energy migrates from monomer to monomer to populate lower energy monomers.

4. Conclusion

The orientation and conformation of RhB18 dye molecules in hybrid Langmuir–Blodgett monolayers containing clay mineral nanoparticles is determined using fluorescence spectroscopy and polarized ATR–FTIR spectroscopy. In films without clay, the phenyl ring of RhB18 is tilted relative to the xanthene plane and both groups are tilted relative to the substrate. No preferential orientation is observed in these films. Films containing clay minerals do show a preferential orientation of RhB18. The phenyl ring and the xanthene plane are parallel to the clay mineral surface and the clay mineral lamellae are parallel to the substrate. The clay surface induces orientational control on the dye molecules in the monolayer. A previous paper showed that the molecular density can be controlled by the surface charge density of the clay minerals.[24] Hybrid Langmuir–Blodgett monolayers containing clay minerals show potential for materials with controlled spatial organization of dye molecules.

Appendix

The spectra of monomers of rhodamine typically undergo a red shift of about 10 nm in a clay mineral dispersion, when compared with a solution spectrum. The monomer of Rh3B (similar structure as RhB18 but with ethyl instead of octadecyl) in an ethanolic solution has a maximum at 556 nm,[47] while the maximum is at 567 nm in a dilute aqueous saponite dispersion.[48] The monomer of RhB18 in ethanol (10^{-6} mol dm^{-3}) absorbs also at 556 nm. We assume that the same red shift of 11 nm occurs for RhB18 in the presence of saponite. Thus, the theoretical monomer absorption spectrum in the LB film can be calculated from the absorption spectrum of RhB18 in ethanol. The spectrum of RhB18 in ethanol is first converted to wavenumbers, then the spectrum is shifted so that the maximum is at 17 637 cm^{-1}. Conversion to wavelength gets the theoretical monomer spectrum of RhB18 on saponite with $\lambda_{max} = 567$ nm (dashed spectrum in Fig. 5a).

To calculate the dimer spectra, this theoretical monomer spectrum is subtracted from the measured spectra (spectra with dotted and solid lines in Fig. 5a) according to eqn. (1).

$$\text{Dimer spectrum} = \text{measured spectrum} - (\text{theoretical monomer spectrum} \times \text{subtraction factor}) \quad (1)$$

The subtraction was performed using the tool 'spectral subtract – autosubtract' in the Grams/32 AI software (Version 6.00). This automated subtraction procedure is based on an iterative algorithm[49,50] which determines the subtraction factor by minimizing the derivative of the resulting dimer spectrum. The derivative is related to the complexity of the spectrum. The measured spectrum is the sum of the monomer spectrum and the dimer spectrum and is thus more complex than the dimer spectrum alone. The absolute area of the first derivative of the calculated dimer spectrum is at minimum when the monomer spectrum is removed from the measured spectrum.

By using this subtraction method, one assumes that the shape of the monomer absorption spectrum remains constant independent of changes in the local environment. Integration of the monomer and dimer spectra from 450 to 650 nm allows the quantification of the amount of monomers in the film relative to the amount of dimers. The obtained integrated areas for each film are plotted in the inset of Fig. 5b.

Acknowledgements

This research is financially supported by the Fund for Scientific Research – Flanders through grant G.0201.02 and the bilateral agreement Flanders – Hungary through grant BIL 00/10 and partly by an IAP program on "Supramolecular Chemistry and Catalysis".

References

1 M. Ogawa and K. Kuroda, *Chem. Rev.*, 1995, **95**, 399–438.
2 G. Schulz-Ekloff, D. Wohrle, B. van Duffel and R. A. Schoonheydt, *Micropor. Mesopor. Mater.*, 2002, **51**, 91–138.
3 J. Bujdák, N. Iyi, Y. Kaneko, A. Czímerová and R. Sasai, *Phys. Chem. Chem. Phys.*, 2003, **5**, 4680–4685.
4 Y. Kaneko, N. Iyi, J. Bujdák, R. Sasai and T. Fujita, *J. Colloid Interface Sci.*, 2004, **269**, 22–25.
5 M. Iwasaki, M. Kita, K. Ito, A. Kohno and K. Fukunishi, *Clays Clay Miner.*, 2000, **48**, 392–399.
6 N. Iyi, R. Sasai, T. Fujita, T. Deguchi, T. Sota, F. López Arbeloa and K. Kitamura, *Appl. Clay Sci.*, 2002, **22**, 125–136.
7 T. Fujita, N. Iyi, T. Kosugi, A. Ando, T. Deguchi and T. Sota, *Clays Clay Miner.*, 1997, **45**, 77–84.
8 T. Endo, T. Sato and M. Shimada, *J. Phys. Chem. Solids*, 1986 **47**, 799–804.
9 M. Pospíšil, P. Čapková, H. Weissmannová, Z. Klika, M. Trchová, M. Chmielová and Z. Weiss, *J. Mol. Model.*, 2003, **9**, 39–46.
10 R. Kaito, K. Kuroda and M. Ogawa, *J. Phys. Chem. B*, 2003, **107**, 4043–4047.
11 I. A. Levitsky, J. Liang and J. M. Xu, *Appl. Phys. Lett.*, 2002, **81**, 1696–1698.
12 Y. Umemura, A. Yamagishi, R. Schoonheydt, A. Persoons and F. De Schryver, *J. Am. Chem. Soc.*, 2002, **124**, 992–997.
13 B. van Duffel, T. Verbiest, S. Van Elshocht, A. Persoons, F. C De Schryver and R. A. Schoonheydt, *Langmuir*, 2001, **17**, 1243–1249.
14 D. Wang, L.-J. Wan, C. Wang and C.-L. Bai, *J. Phys. Chem. B*, 2002, **106**, 4223–4226.
15 V. Tsukanova, H. Lavoie, A. Harata, T. Ogawa and C. Salesse, *J. Phys. Chem. B*, 2002, **106**, 4203–4213.
16 O. N. Slyadneva, M. N. Slyadnev, V. M. Tsukanova, T. Inoue, A. Harata and T. Ogawa, *Langmuir*, 1999, **15**, 8651–8658.
17 T. Inoue, M. Moriguchi and T. Ogawa, *Thin Solid Films*, 1999, **350**, 238–244.
18 K. Ishibashi, O. Sato, R. Baba, D. A. Tryk, K. Hashimoto and A. Fujishima, *J. Colloid Interface Sci.*, 2001, **233**, 361–363.
19 K. Ray and H. Nakahara, *J. Phys. Chem. B*, 2002, **106**, 92–100.
20 M. D. Elking, G. He and Z. Xu, *J. Chem. Phys.*, 1996, **105**, 6565–6573.
21 D. Fischer, W. R. Caseri and G. Hähner, *J. Colloid Interface Sci.*, 1998, **198**, 337–346.
22 G. Lagaly, Layer charge determination by alkylammonium ions, in *Layer charge characteristics of 2 : 1 silicate clay minerals*, ed. A. R. Mermut, Vol. 6 of *CMS Workshop Lectures*, The Clay Minerals Society, Boulder,Colorado, 1994, pp. 1–46.
23 R. A. Vaia, R. K. Teukolsky and E. G. Giannelis, *Chem. Mater.*, 1994, **6**, 1017–1022.
24 R. H. A. Ras, J. Németh, C. T. Johnston, E. DiMasi, I. Dékány and R. A. Schoonheydt, *Phys. Chem. Chem. Phys.*, 2004, **6**, 4174–4184.
25 R. H. A. Ras, C. T. Johnston, E. I. Franses, R. Ramaekers, G. Maes, P. Foubert, F. C. De Schryver and R. A. Schoonheydt, *Langmuir*, 2003, **19**, 4295–4302.
26 R. H. A. Ras, J. Németh, C. T. Johnston, I. Dékány and R. A. Schoonheydt, *Thin Solid Films*, 2004, **466**, 291–294.
27 S. S. Ramos, A. F. Vilhena, L. Santos and P. Almeida, *Magn. Reson. Chem.*, 2000, **38**, 475–478.
28 M. Majoube and M. Henry, *Spectrochim. Acta, Part A*, 1991 **47**, 1459–1466.
29 R. Markuszewski and H. Diehl, *Talanta*, 1980, **27**, 937–946.
30 L. Wang, A. Roitberg, C. Meuse and A. K. Gaigalas, *Spectrochim. Acta, Part A*, 2001, **57**, 1781–1791.
31 I. M. Issa, R. M. Issa, Y. M. Temerk and M. M. Ghoneim, *Egypt J. Chem.*, 1974, **17**, 391–399.
32 H. J. Friedrich, *Z. Naturforsch.*, 1963, **18b**, 635–638.
33 H. Jakobi, A. Novak and H. Kuhn, *Z. Elektrochem. Ber. Bunsen-Ges. Physik. Chem.*, 1962, **66**, 863–870.
34 A. Leifer, D. Bonis, M. Boedner, P. Dougherty, A. J. Fusco, M. Koral and J. E. LuValle, *Appl. Spectrosc.*, 1967, **21**, 71–80.
35 I. López Arbeloa and P. Ruiz Ojeda, *Chem. Phys. Lett.*, 1982 **87**, 556–560.
36 M. Kasha, H. R. Rawls and M. Ashraf El-Bayoumi, *Pure Appl. Chem.*, 1965, **11**, 371–392.
37 E. Vuorimaa, M. Ikonen and H. Lemmetyinen, *Chem. Phys.*, 1994, **188**, 289–302.
38 J. Serratosa, *Am. Miner.*, 1968, **53**, 1244–1251.
39 J. M. Serratosa, *Clays Clay Miner.*, 1966, **14**, 385–391.
40 J. M. Serratosa, *Nature (London)*, 1965, **208**, 679–681.
41 I. Yamazaki, N. Tamai and T. Yamazaki, *J. Phys. Chem.*, 1990, **94**, 516–525.
42 N. Tamai, T. Yamazaki and I. Yamazaki, *Chem. Phys. Lett.*, 1988, **147**, 25–29.
43 D. Pevenage, M. Van der Auweraer and F. C. De Schryver, *Langmuir*, 1999, **15**, 8465–8473.
44 Z. Grauer, D. Avnir and S. Yariv, *Can. J. Chem.*, 1984, **62**, 1889–1894.
45 N. Kato, M. Yamamoto, K. Itoh and Y. Uesu, *J. Phys. Chem. B*, 2003, **107**, 11917–11923.
46 M. Takayanagi, M. Nakata, Y. Ozaki, K. Iriyama and M. Tasumi, *J. Mol. Struct.*, 1997, **405**, 239–246.
47 J. A. B. Ferreira and S. M. B. Costa, *Phys. Chem. Chem. Phys.*, 2003, **5**, 1064–1070.
48 F. López Arbeloa, J. Martínez, J. Bañuelos Prieto and I. López Arbeloa, *Langmuir*, 2002, **18**, 2658–2664.
49 S. Banerjee and D. Li, *Appl. Spectrosc.*, 1991, **45**, 1047–1049.
50 P. C. Gillette and J. L. Koenig, *Appl. Spectrosc.*, 1984, **38**, 334–337.

